High-Energy Al/CuO Nanocomposites Obtained by DNA-Directed Assembly

Fabrice Severac, Pierre Alphonse, Alain Estève, Aurélien Bancaud, Carole Rossi

High Energy Al/CuO nanocomposites obtained by DNA-directed assembly

By *F. Séverac, P. Alphonse, A. Estève, A. Bancaud*,* and *C. Rossi**

[*] Dr. C. Rossi, Dr. F. Séverac, Dr. A. Estève and Dr. A. Bancaud

CNRS; LAAS; 7 avenue du colonel Roche,
F-31077 Toulouse, France
Université de Toulouse; UPS, INSA, INP, ISAE, LAAS ;
F-31077 Toulouse, France
E-mail: rossi@laas.fr, abancaud@laas.fr

Dr. P. Alphonse
CIRIMAT, 118 route de Narbonne,
F-31062 Toulouse, France

Keywords: DNA, self-assembly, nanoenergetic, CuO, Al

Over the next few years, it is expected that new energetic multifunctional materials will be engineered. There is a need for new methods to assemble such materials from manufactured nanopowders. In this article, we demonstrate a DNA-directed assembly procedure to produce highly energetic nanocomposites by assembling Al and CuO nanoparticles into a micron size particle of Al/CuO nanocomposite with exquisite energetic performance in comparison to physically mixed Al/CuO counterparts. Using 80 nm Al nanoparticles, the heat of reaction and the onset temperature are 1.8 kJ/g and 410 °C, respectively. This experimental achievement relies on the development of simple and reliable protocols to disperse and sort metallic and metal oxide nanopowders in aqueous solution and the establishment of specific DNA surface modification processes for Al and CuO nanoparticles. Overall our work, which shows that DNA can be used as structural material to assemble Al/Al, CuO/CuO and Al/CuO composite materials, opens the route for a molecular engineering of the material at the nanoscale.

1. Introduction

Energetic materials store chemical energy that can be released upon thermal, electrical, or optical actuation. These materials are the subject of intense research for military applications,

as well as for civilian purposes, primarily including automotive air bag propellants. Over the last decade, the idea of engineering molecularly built energetic materials with exquisite performances has launched the field of nanoenergetics.[1-3] New classes of nanoenergetic materials, in particular Metastable Intermolecular Composites (MIC) or thermite nanocomposites, which are composed of oxidizer and fuel nanoparticles with typical particle sizes spanning tens to hundreds of nanometers, constitute a promising option for the development of propellants and explosives. So far MIC have been predominantly prepared by physical mixing of powders, using aluminum nanoparticles (NPs) as fuel, and various oxidizers including MoO_3, CuO, Fe_2O_3 and Bi_2O_3.[4-9] These investigations unambiguously established that thermite nanocomposite ignition and combustion properties can be affected by varying the size of their constituents and their intimacy.[4, 5, 7-17] For instance decreasing the size of nanoparticles enhances the combustion rate, and lowers the ignition temperature. Moreover, the arrangement of oxidizer and fuel nanoparticles and their intimacy significantly impact nanothermite burn rate, and determine the propagation rate of combustion wave front and the release of energy. As a consequence, it has been demonstrated experimentally that the maximum interfacial contact area between the oxidizer and the fuel is necessary to achieve optimal energetical performances. However, the preparation of nanothermite by physical mixing does not allow controlling the arrangement of NPs at the nanoscale.

Self assembly techniques have been vaunted as a cutting-edge solution to precisely engineer the 3D organization of NPs, and hence optimize the energetical properties of nanothermite. Nanostructured composites were for instance obtained by electrostatic self assembly based on oppositely charging Al and Fe_2O_3 NPs in aerosol,[18] or by functionalization of Al and CuO NPs with oppositely charged ligands.[19] Alternatively nanothermite composed of CuO nanorods and Al NPs were assembled using poly(4-vinylpyridine) as assembly material.[20] These different methods allowed to generate micron sized nanothermites characterized by highly energetic performances. In another direction, DNA-directed assembly, which consists

in coating two types of nanoparticles with single stranded DNAs of complementary sequences in order to direct the aggregation of NPs has the unique potential to generate DNA-programmable NPs crystals[23]. So far this approach, which relies on the spontaneous formation of DNA double helix held together by hydrogen bonds between complementary base pairs,[21, 22] has mostly been performed with gold and silver NPs, and applied to biodetection or plasmonic applications.[21-25] While these NPs can be considered as well-defined model systems for fundamental research, the potential of DNA-directed assembly technology for other nanomaterials and applicative areas remains to be demonstrated and further explored.

In this paper, we add a new material to the already rich palette of applications of DNA-directed assembly technology by fabricating high performance nanoenergetic materials. For this, specific approaches to disperse Al and CuO colloids from nanopowders are established, and different coating strategies with single stranded DNA are validated. DNA directed Al/CuO nanocomposite assembly kinetics are then monitored in real time, and the intimacy of NPs arrangement in the resulting thermite nanocomposite is investigated by energy dispersive X-ray analysis. The energetic performances of the material in terms of onset temperature and heat of reaction are assessed quantitatively and compared to the literature, showing a significantly higher heat of reaction compared to physical and randomly mixed thermite nanocomposites.

2. Results and discussion

Al/CuO nanocomposites assembly procedure is presented in **(Fig. 1)**. CuO and Al NPs were purchased as solid powders, dispersed/sorted in aqueous environment, and functionalized with short single-stranded DNAs. These successive steps are first validated, and the assembly of nanothermite is subsequently investigated.

2.1. Dispersion and surface modification of Al and CuO colloids

CuO and Al powders of nominal sizes 50 nm, and 80 nm or 120 nm, respectively, were dispersed in ultrapure water containing 0.1% surfactant (Tween 20) as a stabilization agent. These solutions were buffered at pH=7 because copper oxide and aluminum oxide, which spontaneously forms a ~3 nm passivation shell around Al NPs, are neither oxidized nor reduced in neutral conditions.[26, 27] They were then sonicated for 3 minutes (see Methods) in order to obtain colloidal solutions of mean hydrodynamic diameters of 185+/-40 nm, 180+/-60 nm, and 210+/-70 nm for 50 nm CuO, 80 nm Al, and 120 nm Al NPs, respectively, as inferred from dynamic light scattering (DLS ; inserts of **(Fig. 2a-b)**). The resulting colloidal solutions were thus composed of small aggregates of ~2-4 NPs, as directly confirmed by scanning electron microscopy (see **(Fig. S1)** supporting information). These particles were stable in aqueous conditions over hours, as demonstrated by the constant hydrodynamic diameter derived from DLS **(Fig. 2a-b)**. Notably, we observed that longer periods of sonication did not reduce the size of these aggregates, and rather produced colloidal suspensions of larger dimensions (supporting information **(Fig. S2)**).

The grafting strategy of single stranded DNA on CuO and Al NPs was first tackled by density functional theory (DFT) modeling. As in the well-known case of Au surfaces, thiol moieties, which are organosulfur compounds (-SH), react with CuO surfaces to form a Cu-S bond characterized by a gain in energy of -1.51 eV; this is quantitatively even more favourable than in the case of Au-S bond formation, which is accompanied with an exothermic reaction pathway of -0.93 eV. The grafting mechanism is associated with the intrinsic ability of CuO to be reduced by thiol moieties through the concomitant formation of sulfonic acids ($-SO_3H$) or H_2O with exothermic energy budgets of -0.84 and -1.27 eV, respectively. These results are in keeping with protocols established for the formation of self-assembled monolayers on copper oxide surfaces.[28-31] The reducing properties of thiol moieties are no longer valid for

oxidized aluminum that exhibits an endothermic energy profile (+0.29 eV). Consequently two different strategies to graft single stranded DNA on CuO and Al NPs have to be developed.

On the one hand, CuO NPs were functionalized with thiol modified oligonucleotides (see Methods), systematically showing a small increase in hydrodynamic diameter of ~10 nm **(Fig. 2a)**. Given that oligonucleotides measure 4 nm according to DLS (data not shown), the presence of DNA at the surface of NPs is expected to increase their hydrodynamic diameter by ~8 nm, in keeping with our estimates. The surface modification of CuO NPs with DNA was also confirmed by the detection of a change in surface potential of -9 mV (Table in **(Fig. 2c)**). Finally, beyond the testimony of the successfully modification of CuO NPs with DNA, DLS measurements provide a direct evidence that CuO colloids remain stable in water after DNA modification during at least 1 h **(Fig. 2a)**.

On the other hand, the amphoteric nature of alumina surfaces and the high stability of its Al-O constituents led us to develop a strategy based on the non specific binding of neutravidin to aluminum oxide (see details in Methods).[32, 33] Neutravidin is a tetrameric protein that forms one of the strongest non covalent bond with biotin, which is a small vitamin that can be coupled to virtually any biomolecules.[35] We observed that the adsorption of neutravidin to Al NPs induces a positive shift in surface potential of +14 mV, together with an increase in hydrodynamic diameter of 15 nm **(Fig. 2d and b)**. These two trends are consistent with the formation of an homogeneous protein layer because (i) neutravidin is a neutral protein at neutral pH, and (ii) the diameter of avidin (a neutravidin analog) is ~7 nm according to X-ray crystallography.[34] We then added oligonucleotides chemically linked to biotin, which appeared to bind to neutravidin coated Al NPs, as inferred from the negative departure of the surface potential, and the increase in hydrodynamic diameter of 15 nm **(Fig. 2d and b)**. Given that we deal with NPs of similar size, consistent zeta potentials for DNA coated Al and CuO NPs indicate that roughly similar DNA grafting densities have been reached for both types of NPs.

2.2. Assembly of CuO/CuO, Al/Al and Al/CuO thermite nanocomposites

Next, we focus on the mechanism of DNA directed assembly of both Al and CuO NPs. The aggregation kinetics, as inferred from the mean hydrodynamic diameter, was monitored in real time using DLS, and the pivotal role of DNA in the assembly was assayed by comparing the effect of complementary and non-complementary strands (for example ssA+ssB and ssA+ssC in **(Table 1)**, respectively). The hydrodynamic diameter of CuO/CuO, Al/Al and Al/CuO mixtures, which were mixed in stoichiometric ratio, remains constant over time at ~200 nm with non complementary strands (lower datasets in **(Fig. 3a-b-c)**). In contrast NPs coated with complementary strands tend to aggregate, and CuO/CuO, Al/Al and Al/CuO nanocomposites of several microns are obtained within a few hours (upper datasets in **(Fig. 3a-b-c)**), as confirmed by scanning electron microscopy images, which show the existence of 1.9 µm compact Al/CuO aggregates composed of hundreds of Al and CuO individual NPs **(Fig. 4a)**. Moreover, the aggregation kinetics follows a non linear temporal response, which is accurately fit with a power law function (solid lines in **(Fig. 3a-b-c)**). Interestingly the non linear growth rate for Al/Al, CuO/CuO, and Al/CuO aggregates is characterized by exponents of 0.57+/-0.01, 0.54+/-0.01, and 0.49+/-0.02, respectively. This scaling is consistent with the exponent of 0.56 observed for the formation of diffusion-limited aggregates,[36] which are obtained when the assembly dynamics is limited by NPs diffusion. We then tested this interpretation by performing another experiment, in which CuO and Al NPs were coated with non-complementary strands (ssA and ssC_b). A linker, which is complementary to ssA and ssC_b **(Table 1)**, was subsequently added in excess to completely coat the surfaces of Al and CuO NPs, and impede the rapid formation of bridges between them as in the mechanism of diffusion-limited aggregation. Note that bridges between NPs eventually form because the association of the linker between the two ssA and ssC_b strands is more stable thermodynamically. The assembly kinetics was expectedly slowed down (middle dataset in

(Fig. 3c)). Moreover the aggregation growth rate became linear, this signature being characteristic of reaction-limited kinetics.[37] Consequently, our results demonstrate the successful fabrication of Al/CuO nanocomposites by DNA directed assembly, and that the assembly kinetics can be monitored with different DNA assembly strategies.

2.3. Characterization and performances of DNA assembled Al/CuO thermite nanocomposites

DNA assembled Al/CuO thermite nanocomposites were subsequently analyzed at the individual aggregate level by energy dispersive X-ray analysis (EDX) in conjunction with SEM **(Fig. 4)**. The coarse-grained EDX energy spectrum of the cluster shown in **(Fig. 4b)** indicates the presence of NPs structural elements, namely copper, aluminum and oxygen, as well as an expected peak of phosphorus due to the presence of DNA in the aggregate **(Fig. 4a)**. Thus, our assembly strategy enables to obtain random aggregates of Al and CuO NPs, and the the EDX spectrum qualitatively shows that Al and Cu are present in equivalent proportions of 33% and 31%, respectively (the percents of the other atomic elements are 16%, 5%, 14%, and 1% for O, P, Ni and C, respectively). This result was further supported by mapping the presence of Al and Cu in individual clusters by performing spatially resolved EDX analysis **(Supplementary Fig. S3)**, which directly demonstrated the presence of Al and CuO NPs in small aggregates. Al/CuO nanocomposites thermal properties were then characterized by Differential Scanning Calorimetry (DSC; see methods). In a first set of experiments, the thermal decomposition of physically-mixed and DNA-assembled Al/CuO nanocomposites was compared (see **(Fig. 5)**). Al and CuO NPs were dispersed from the same commercial powders and stabilized in the same conditions (see methods), and both materials released heat upon thermal actuation. Yet the heat of reaction is greatly enhanced for DNA-assembled nanocomposites, as demonstrated by the total heat of reaction of 1500 J/g *vs*. 200 J/g starting from 560 °C for the DNA-assembled *vs*. physically-mixed Al (120 nm)/CuO nanothermite,

respectively (dashed areas in **(Fig. 5)**). Notably these heats of reaction are lower than the theoretical maximum of 3900 J/g most likely because of the existence of a thin passivation oxide layer around Al NPs, [38] as well as the presence of DNA at the interface between Al and CuO. Nevertheless, we clearly establish that DNA directed assembly of thermite nanocomposite results in enhanced energy release. Next we investigated whether the size of Al NPs changed the onset temperature and the heat of reaction. The thermal decomposition DNA-assembled Al/CuO thermite nanocomposites made from 120 nm *vs*. 80 nm Al NPs was compared using the same preparation protocol and stoichiometric. The integration of the exotherm indicates an increased total heat of reaction of 1800 J/g for 80 nm Al NPs *vs.* 1500 J/g for 120 nm NPs. Interestingly, the measured heat of reaction (1800 J/g) and onset temperature (410°C) are among the best ever achieved for thermite nanocomposites. Indeed, maximal performances were obtained using electrostatic NPs assembly of Al and Fe_2O_3, yielding a comparable heat of reaction of 1800 J/g, that is 46% of the theoretical value.[38] Our results also outperform the results obtained by physical mixing of Al/MoO_3 nanothermite,[39] or by multilayering Al/CuO nanothermites,[40] both methods yielding a heat of reaction of 1200 J/g. We also demonstrate that the onset temperature is reduced from 470 °C to 410 °C using 80 nm Al NPs instead of 120 nm NPs. Beyond the fact that this onset temperature is to our knowledge the lowest published in the literature, our result suggests that the ignition threshold can be tuned with Al NPs size while keeping the same assembly protocol. Interestingly this trend was also observed in earlier contributions, though based on drastic comparisons of Al nano- *vs.* micro- particles. For instance a reduction of the ignition temperature from 955 °C to 476 °C was demonstrated with Al/MoO_3 thermite composite containing 40 nm *vs.* 10 µm Al particles, respectively.[41] These results are consistent with the onset temperature of 460 °C measured for Al/MoO_3 obtained with Al NPs of 52 nm.[39] In a similar direction, Granier and Pantoya examined the ignition sensitivity of thermite composites using Al nano- and micro-particles mechanically mixed with MoO_3,[42] and

demonstrated ignition delay times two orders of magnitude lower for thermite nanocomposites. Interestingly though, the ignition delay remained unchanged for Al NPs of 50 nm and 100 nm using Al/CuO or Al/MoO_3 nanothermites.[42,43]

The low level of the onset temperature obtained in our experiments may first be explained by the fact that Al NPs exhibit an increased surface energy that was shown to be associated to a reduced Al melting temperature in comparison to large aluminum particles.[44,45] This behavior has been attributed to (i) the expansion of the Al core upon heating that breaks the alumina shell, and leads to the ejection of small molten clusters of Al at high velocity[47]; or (ii) to the diffusion of Al atoms through physical cracks in the shell.[48, 49] Moreover, after the ignition threshold, DSC curves are characterized by a smooth profile, which indicates a lower reaction kinetics. Interestingly, the presence of carbon on the DNA strands surrounding NPs may account for this low combustion rate, as well as for the lower the onset temperature. Indeed, it was shown that the addition of the burning of carbon nanofibers occurred at 300°C in contact with MnO_2, and that the combustion velocity of Al/MnO_2 nanothermites was reduced from 730 to 5 mm/s by adding 37 % in weight of carbon nanofibers.[50] It is also tempting to invoke that the potential concurrent reaction of Al with carbon ($4Al + 3C \rightarrow Al_4C_3$) could contribute to the lower the reaction exothermicity.

3. Conclusions

This paper reports on DNA-based bottom-up nanofabrication of Al and CuO NPs into a micron size particle of Al/CuO thermite nanocomposite with exquisite and tunable energetic performance in comparison to physically mixed counterparts. This achievement has been reached owing to efforts to stabilize Al and CuO colloids obtained from commercial nanopowders in aqueous environment. As validated by DFT calculations, two strategies were followed to bind oligonucleotides on Al and CuO NPs: thiol-modified oligonucleotides were

attached to copper oxide NPs and biotin-neutravidin system was employed to coat aluminum NPs. In the first case, the strong affinity of thiol groups for copper oxide allows to directly graft thiol modified oligonucleotides to CuO NPs. In the second case, neutravidin is adsorbed on the thin alumina shell covering the aluminum NPs, and biotin modified oligonucleotides are grafted on these protein modified NPs. Micron sized self-assembled Al/CuO energetic nanocomposites were eventually obtained through DNA hybridization.

We have characterized the resulting Al/CuO nanothermites by Differential Scanning Calorimetry, showing a total heat of reaction of 1800 J/g for "80 nm" Al NPs, which is among the best ever achieved. We also demonstrated the possibility to tune the onset temperature by changing the size of aluminum NPs while keeping the same assembly protocol. Our methodological study, which does not yet provide the complete spectrum of characterizations (combustion velocity, ignition delay, etc…) to fully document the potential of DNA-assembled energetic materials and to reach optimal performances, thus paves the way to a new route to fabricate nanothermite with a precise control on the material assembly reaction.

Interestingly, this strategy to assemble high energetic nanothermite composite may enrich a number of applications in nanoenergetics including environmentally clean primers, miniature safe detonators, thermal batteries, in-situ welding, soldering, and chemical agent neutralization. ie thus assembled nanothermite composite can be integrated in a portable apparatus to generate high temperature (2000°C - 3000°C) for molecule degradation applicable to neutralize mustard agent for example. Another possibility is to produce ions (Cu+, Al+, NOx+) from the thermite reaction to provide effective pH control for chemical neutralization locally. Or specific chemical Species could be also generated by grafting specific molecules with nanothermite during assembly process. In longer term, we envision that the DNAs strands that direct NPs assembly can bear additional chemical, biological, or physical cues to generate multifunctional energetic nanocomposites. For instance, the information encoded in the DNA strands may be exploited by incorporating specific

sequences recognized by e.g. restriction enzymes[46] to trigger the irreversible dissociation of energetic materials for safely unloading fire devices. In another direction, absorbing dyes may be integrated in the DNA backbone in order to trigger energy release through light exposure. Finally, we posit that individual NPs can be functionalized with multiple DNA strands in order to assemble materials optimized to release heat as well as e.g. gas for the generation of new propellants. Altogether DNA assembly thus appears to open new avenues toward the fabrication of multifunctional energetic materials.

4. Experimental

4.1. Chemicals

50 nm copper oxide (CuO) and 120 nm or 80 nm aluminum (Al) nanopowders were purchased from PlasmaChem GmbH and Novacentrix, respectively. Al NPs purity is 75% from manufacturer data leading to an alumina shell thickness ranging from 3.3 to 5 nm (see **Fig. S4** in supporting information). All chemical reagents were purchased from Sigma-Aldrich, and oligonucleotides **(Table 1)** were purchased from Eurogentec. DNA concentrations were systematically evaluated by UV-visible spectroscopy using a Nanodrop 2000C spectrophotometer. All experiments were carried out with 1.5 mL hydrophobic microtubes to prevent unspecific adsorption on surfaces.

4.2. General methods

Sonication. 40 mg of nanopowders were suspended in 50 mL of 0.1 M PBS + 0.1% Tween-20, and colloids were sonicated using a Vibra-Cell VCX 500 ultrasonic probe system at 200 W during 3 minutes with 2 s pulses separated by 1 s. Notably, the surfactant Tween-20 was selected because it does not interfere with the interaction properties of biomolecules, and in particular with the biotin-streptavidin binding reaction.

Dynamic Light Scattering and zeta potential measurements. A Zetasizer Nano ZS (Malvern Instruments) was used to determine NPs hydrodynamic diameter by DLS, and zeta potential by Doppler laser electrophoresis. All zeta-potential measurements were performed in water, and the temperature was maintained at 25 °C.

Scanning electron microscopy (SEM). The samples were thoroughly rinsed 5 times with a volatile salt (20 mM ammonium acetate) before SEM imaging, which was performed on a Hitashi S4800 coupled to an energy-dispersive X-ray spectroscopy system (EDX). Samples were prepared by depositing and evaporating a droplet of the aqueous colloidal solution on a carbon-coated nickel grid.

Differential Scanning Calorimetry. Differential Scanning Calorimetry measurements were performed on a SETARAM DSC 111G system under nitrogen flow with a Supelco super clean gas purifier oxygen trap over a temperature range from 300 K to 1000 K and an heating rate of 5 K/min. Samples were transferred and evaporated in an alumina crucible for thermal analysis.

4.3. DNA modified CuO NPs preparation

The terminal sulfur atoms of thiolated DNA tend to form dimers in solution. Prior to use, thiolated DNAs were thus deprotected by cleaving disulfide bonds using 0.1 M of dithiothreitol (DTT) dissolved in PBS during 1 hour. DTT was then removed using a desalting NAP-5 column (GE Healthcare), and freshly deprotected thiolated oligonucleotides were added to CuO colloids at a final concentration of 3 µM. This mixture was left overnight on a microtube rotator to prevent sedimentation. The solution was then buffered to 10 mM phosphate (NaH_2PO_4/Na_2HPO_4) and to 0.1 M NaCl by dropwise addition of 2 M NaCl solution. After 24 h, excess DNA was eventually removed by multiple centrifugations at 14.000 rpm (5 min), and NPs were resuspended in 0.3 M PBS to conduct assembly experiments.

4.4. DNA modified Al NPs preparation

6 µl of neutravidin (1 mg/ml) was added to 1 mL of sonicated Al NPs during 30 minutes. The excess of reagent was removed by 5 centrifugations at 14.000 rpm (5 min), and neutravidin coated NPs were resuspended in 0.1 M PBS. Then, biotin-modified oligonucleotides were added at a final concentration of 3 µM, and allowed to stand for 2 hours on the microtube rotator. DNA coated NPs were eventually rinsed as described for CuO NPs with 0.3 M PBS. Interestingly, we noted that Al NPs were stable in 0.3 M PBS + 0.1% tween-20 during weeks, whereas particles were oxydized in a few days when dispersed in ultrapure water.

4.5. Preparation of physically-mixed Al-CuO composites

40 mg of unmodified 120 nm Al and CuO nanopowders were suspended in 50 mL of ultrapure water supplemented with 0.1% Tween-20. This mixture was then suspended using ultrasonic waves during 3 minutes as described in 4.2.

[1] *The AMPTIAC Newsletter* **2002**, *6*.

[2] S. F. Son, R. Yetter., V. Yang., *Journal of Propulsion and Power* **2007**, *23*, 643.

[3] C. Rossi, A. Estève, P. Vashishta, *Journal of Physics and Chemistry of Solids* **2010**, *71*, 57.

[4] B. S. Bockmon, M. L. Pantoya, S. F. Son, B. W. Asay, J. T. Mang, *Journal of Applied Physics* **2005**, *98*, 064903.

[5] T. Foley, A. Pacheco, J. Malchi, R. Yetter, K. Higa, *Propellants, Explosives, Pyrotechnics* **2007**, *32*, 431.

[6] M. L. Pantoya, J. J. Granier, *Journal of Thermal Analysis and Calorimetry* **2006**, *85*, 37.

[7] E. V. Sanders, B. W. Asay, T. Foley, B.C. Tappan, A. Pacheco, S. F. Son, *Journal of propulsion and power* **2007**, *23*, 8.

[8] M. Schoenitz, S. Umbrajkar, E. Dreizin, *Journal of propulsion and power* **2007**, *23*, 5.

[9] S. F. Son, B. W. Asay, T. Foley, R. Yetter, M. Wu, G. Risha, *Journal of propulsion and power* **2007**, *23*, 7.

[10] R. Armstrong, N. Thadhani, W. Wilson, J. Gilman, R. E. Simpson, *Mat Res Soc Symp Proc* **2003**, *800*.

[11] C. E. Aumann, G. L. Skofronick, J. A. Martin, *The 3rd International Conference on Nanometer-Scale Science and Technology* **1995**, *13*, 1178.

[12] S. H. Fischer, M. C. Grubelich, *AIAA* **1996**.

[13] M. L. Pantoya, J. J. Granier, *The effect of slow heating rates on the reaction mechanisms of nano and micron composite thermite reactions*, Springer, Dordrecht, PAYS-BAS **2006**.

[14] M. L. Pantoya, J. J. Granier, *ibid* **2005**, *30*, 53.

[15] J. A. Puszynski, C. J. Bulian, J. J. Swiatkiewicz, *Journal of propulsion and power* **2007**, *23*, 9.

[16] N. Thadhani, R. Armstrong, A. Gash, W. e. Wilson, *Mat Res Soc Symp Proc* **2006**, *57*.

[17] K. C. Walter, D. R. Pesiri, D. E. Wilson, *Journal of propulsion and power* **2007**, *23*, 6.

[18] S. H. Kim, M. R. Zachariah, *Advanced Materials* **2004**, *16*, 1821.

[19] J. Y. Malchi, T. J. Foley, R. A. Yetter, *ACS Applied Materials & Interfaces* **2009**, *1*, 2420.

[20] R. Shende, S. Subramanian, S. Hasan, S. Apperson, R. Thiruvengadathan, K. Gangopadhyay, S. Gangopadhyay, P. Redner, D. Kapoor, S. Nicolich, W. Balas, *Propellants, Explosives, Pyrotechnics* **2008**, *33*, 239.

[21] C. A. Mirkin, *Inorganic Chemistry* **2000**, *39*, 2258.

[22] C. A. Mirkin, R. L. Letsinger, R. C. Mucic, J. J. Storhoff, *Nature* **1996**, *382*, 607.

[23] S. Y. Park, A. K. R. Lytton-Jean, B. Lee, S. Weigand, G. C. Schatz, C. A. Mirkin, *Nature* **2008**, *451*, 553.

[24] R. C. Mucic, J. J. Storhoff, C. A. Mirkin, R. L. Letsinger, *Journal of the American Chemical Society* **1998**, *120*, 12674.

[25] C. J. Loweth, W. B. Caldwell, X. Peng, A. P. Alivisatos, P. G. Schultz, *Angewandte Chemie International Edition* **1999**, *38*, 1808.

[26] T. Hagyard, J. R. Williams, *Transactions of the Faraday Society* **1961**, *57*, 2288.

[27] R. S. Alwitt, J. W. Dekker, *New York* **1976**, *4*, 169.

[28] D. L. Allara, R. G. Nuzzo, *Langmuir* **1985**, *1*, 52.

[29] D. L. Allara, R. G. Nuzzo, *Langmuir* **1985**, *1*, 45.

[30] J. P. Folkers, C. B. Gorman, P. E. Laibinis, S. Buchholz, G. M. Whitesides, R. G. Nuzzo, *Langmuir* **1995**, *11*, 813.

[31] P. E. Laibinis, G. M. Whitesides, D. L. Allara, Y. T. Tao, A. N. Parikh, R. G. Nuzzo, *Journal of the American Chemical Society* **1991**, *113*, 7152.

[32] J. Korlach, P. J. Marks, R. L. Cicero, J. J. Gray, D. L. Murphy, D. B. Roitman, T. T. Pham, G. A. Otto, M. Foquet, S. W. Turner, *Proceedings of the National Academy of Sciences* **2008**, *105*, 1176.

[33] H. Susmita, D. Chattoraj, K., *Protein adsorption at solid-liquid interfaces. I, affinities of protein for alumina surface*, Vol. 28, Council of Scientific & amp; Industrial Research, New Delhi, INDE **1991**.

[34] J. A. E. Määttä, T. T. Airenne, H. R. Nordlund, J. Jänis, T. A. Paldanius, P. Vainiotalo, M. S. Johnson, M. S. Kulomaa, V. P. Hytönen, *ChemBioChem* **2008**, *9*, 1124.

[35] E. P. Diamandis, T. K. Christopoulos, *Clin Chem* **1991**, *37*, 625.

[36] D. A. Weitz, J. S. Huang, M. Y. Lin, J. Sung, *Physical Review Letters* **1984**, *53*, 1657.

[37] S. Cobbe, S. Connolly, D. Ryan, L. Nagle, R. Eritja, D. Fitzmaurice, *The Journal of Physical Chemistry B* **2002**, *107*, 470.

[38] S. H. Fischer, M. C. Grubelich, *Proceedings of the 24th International Pyrotechnics Seminar, Monterey, CA* **27-31 July 1998**.

[39] J. Sun, M. L. Pantoya, S. L. Simon, *Thermochimica Acta* **2006**, *444*, 117.

[40] M. Petrantoni, C. Rossi, L. Salvagnac, V. Conedera, A. Esteve, C. Tenailleau, P. Alphonse, Y. J. Chabal, *Journal of Applied Physics* **2010**, *108*, 084323.

[41] M. L. Pantoya, J. J. Granier, *ibid* **2005**, *30*, 53.

[42] J. J. Granier, M. L. Pantoya, *Combustion and Flame* **2004**, *138*, 373.

[43] C. J. Bulian, T. T. Kerr, J. A. Puszynski, *31st Proc. Int. Pyrotech. Seminar* **2004**, 327.

[44] J. Eckert, J. C. Holzer, C. C. Ahn, Z. Fu, W. L. Johnson, *Nanostructured Materials* **1993**, *2*, 407.

[45] C. R. M. Wronski, *British Journal of Applied Physics* **1967**, *18*, 1731.

[46] A. G. Kanaras, Z. Wang, A. D. Bates, R. Cosstick, M. Brust, *Angewandte Chemie* **2003**, *115*, 201.

[47] V.I. Levistas, B.W. Asay, S.F. Son, M. Pantoya, *J. Appl. Phys.* **2007**, 101, 083524

[48] A. Rai, K. Park, L. Zhou, M.R. Zachariah, *Combust. Theory Modell*. **2006**, 10,843

[49] B.J. Henz, T. Hawa, M.R. Zacharia, *J. Appl. Phys*. **2010**,107, 024910

[50] B. Siegert, M. Comet, O. Muller, G. Pourroy, D. Spitzer , *J. Phys. Chem*. **2010**, 114, 19562-19568

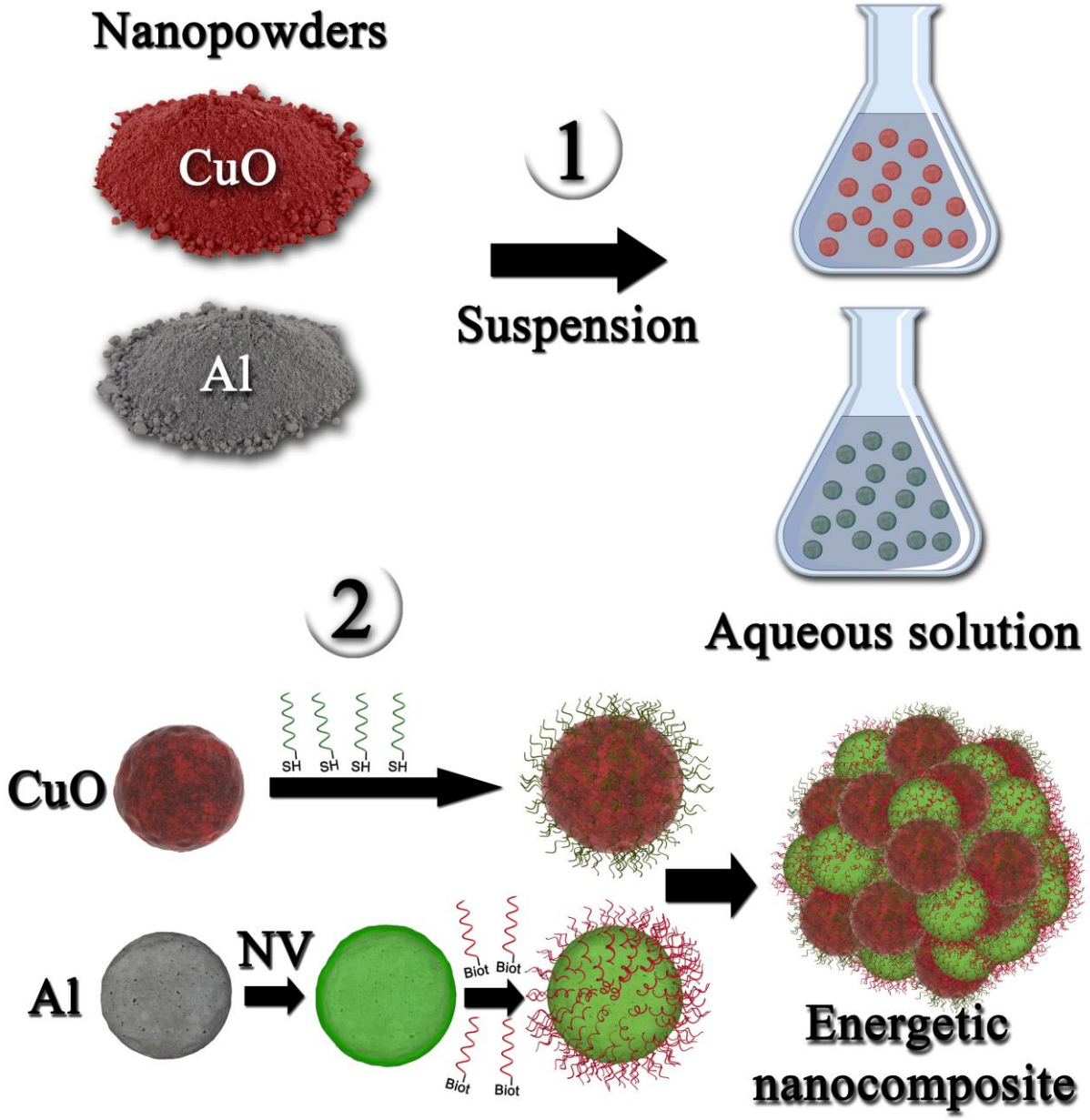

Figure 1. Schematics of the different steps for the DNA-directed assembly of Al/CuO thermite nanocomposites. Aluminum and copper oxide nanopowders are first suspended and stabilized in aqueous solution, then functionalized with single DNA strands, and eventually assembled through hybridization of complementary DNA strands.

(a)

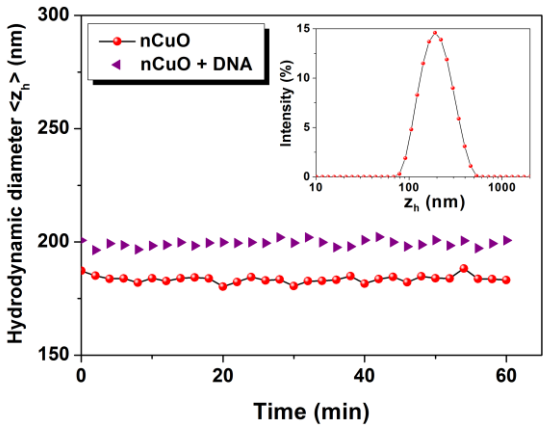

(b)

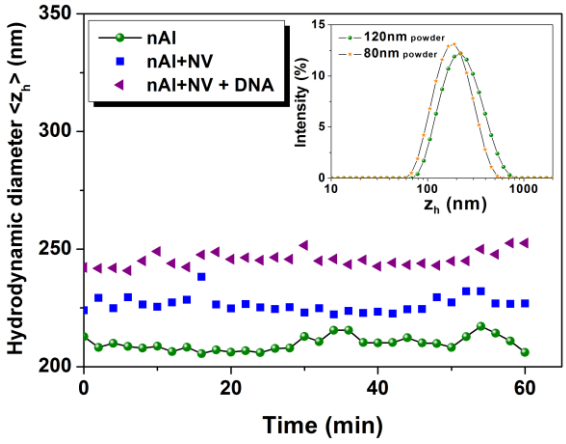

(c)

	Zeta-potential (mV)	Deviation
nCuO	-13	± 5
nCuO+DNA	-22.4	± 5.1

(d)

	Zeta-potential (mV)	Deviation
nAl	-22.6	± 5.1
nAl + NV	-8.2	± 5.7
nAl + NV + DNA	-23.1	± 7.2

Figure 2. Stabilization and surface modification of Al and CuO colloids. (a) The average hydrodynamic diameter of CuO nanoparticles suspended in aqueous solution is measured by DLS before and after DNA functionalization (red and purple datasets, respectively). The inset shows the size distribution of CuO colloids before surface modification. (b) The average hydrodynamic diameter of 120 nm Al nanoparticles is measured by DLS suspended in aqueous solution, after the neutravidin coating, and DNA grafting (green, blue, and purple datasets, respectively). The inset shows the size distribution of 80 nm and 120 nm Al colloids before surface modification (orange and green, respectively). (c-d) The zeta potential of CuO and Al nanoparticles is measured at the different steps of the process.

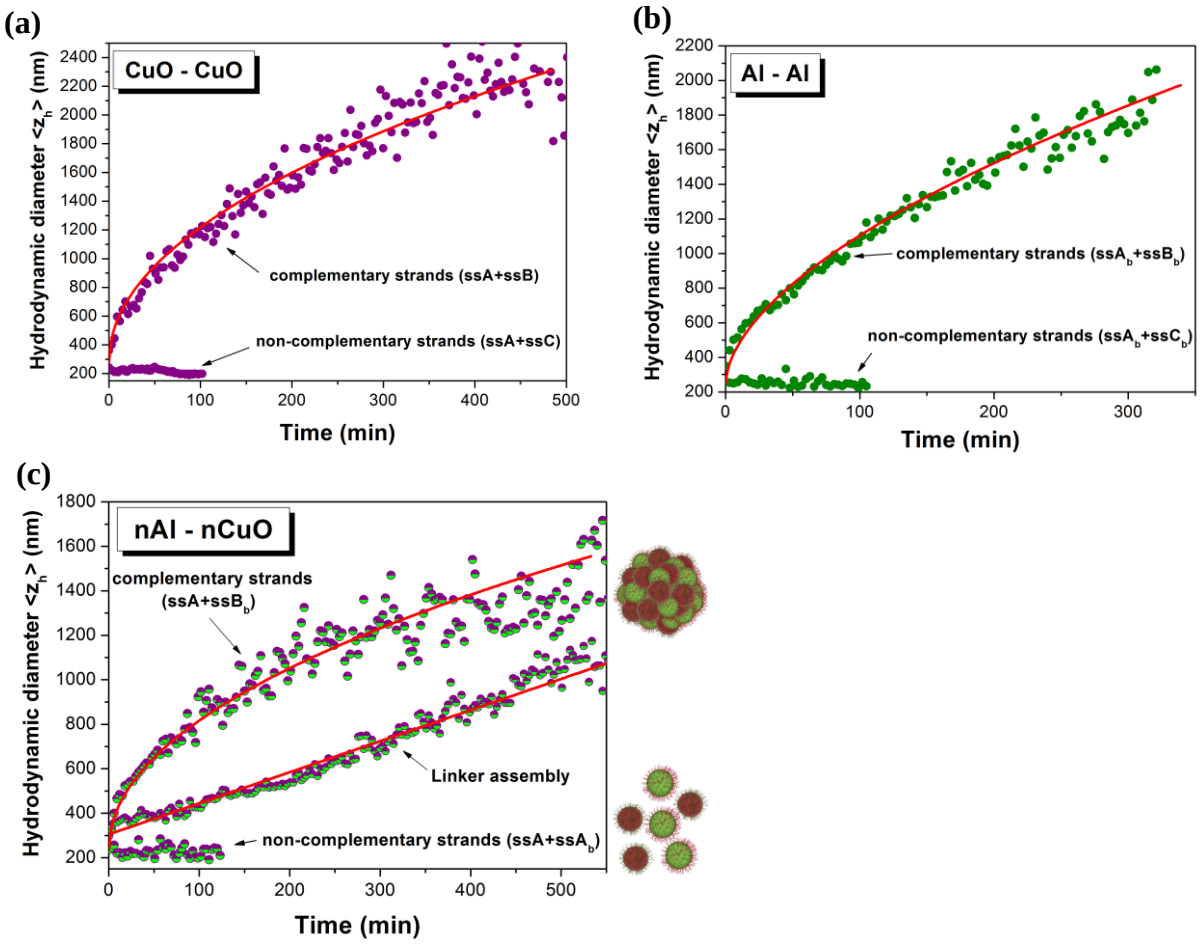

Figure 3. Real time assembly kinetics of Al and CuO nanoparticles. The mean hydrodynamic diameter of DNA-coated CuO+CuO (a), Al+Al (b), and Al+CuO (c) colloidal solutions is monitored in real time, showing that aggregation does not occur with non complementary strands (lower datasets in each graph), and instantly starts with complementary oligonucleotides. Red lines represent fits of the kinetics with non linear or linear temporal responses.

(a)

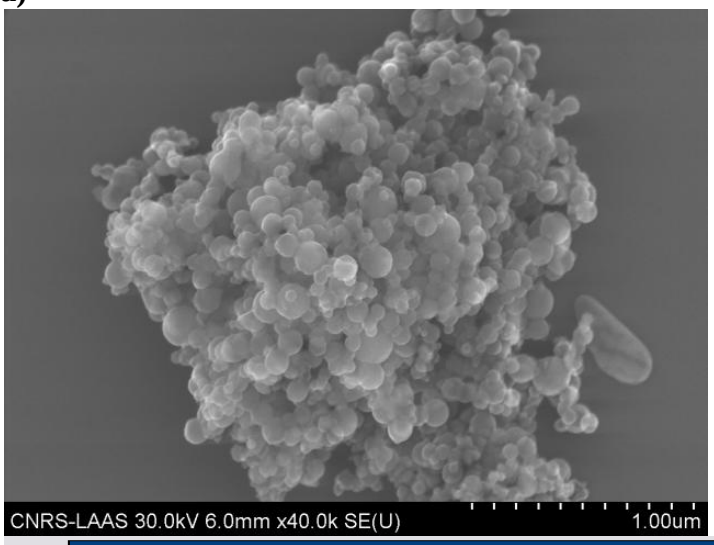

(b)

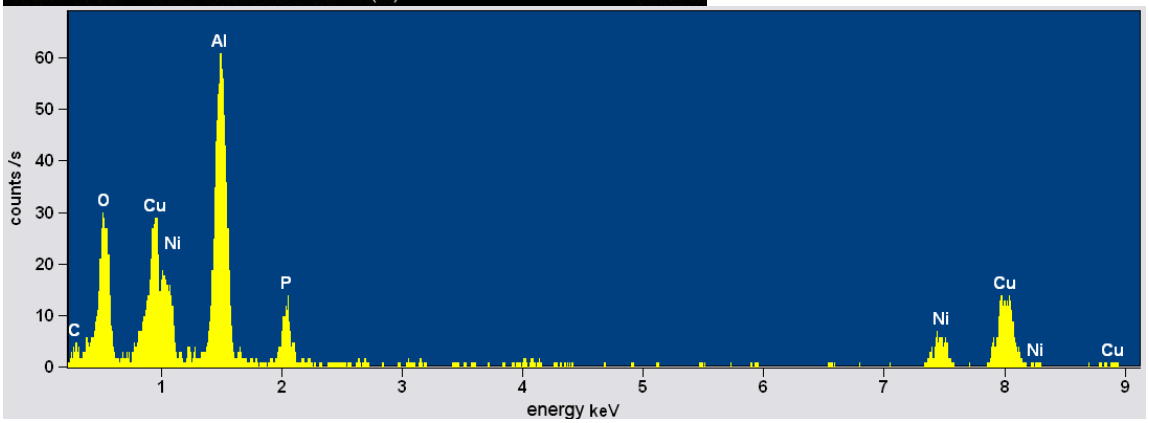

Figure 4. Structural characterization of DNA assembled Al/CuO thermite nanocomposites. (a) Scanning electron micrograph of one individual Al/CuO aggregate of ~2µm. (b) The composition of the ag gregate shown in (a) is investigated by energy dispersive X-ray analysis (EDX), showing the presence of Al, Cu, and O, as well as phosphorus (P) due to the presence of DNA in the aggregate. Note that Carbon and Nickel are also detected because of the use of carbon-coated nickel grids for SEM imaging.

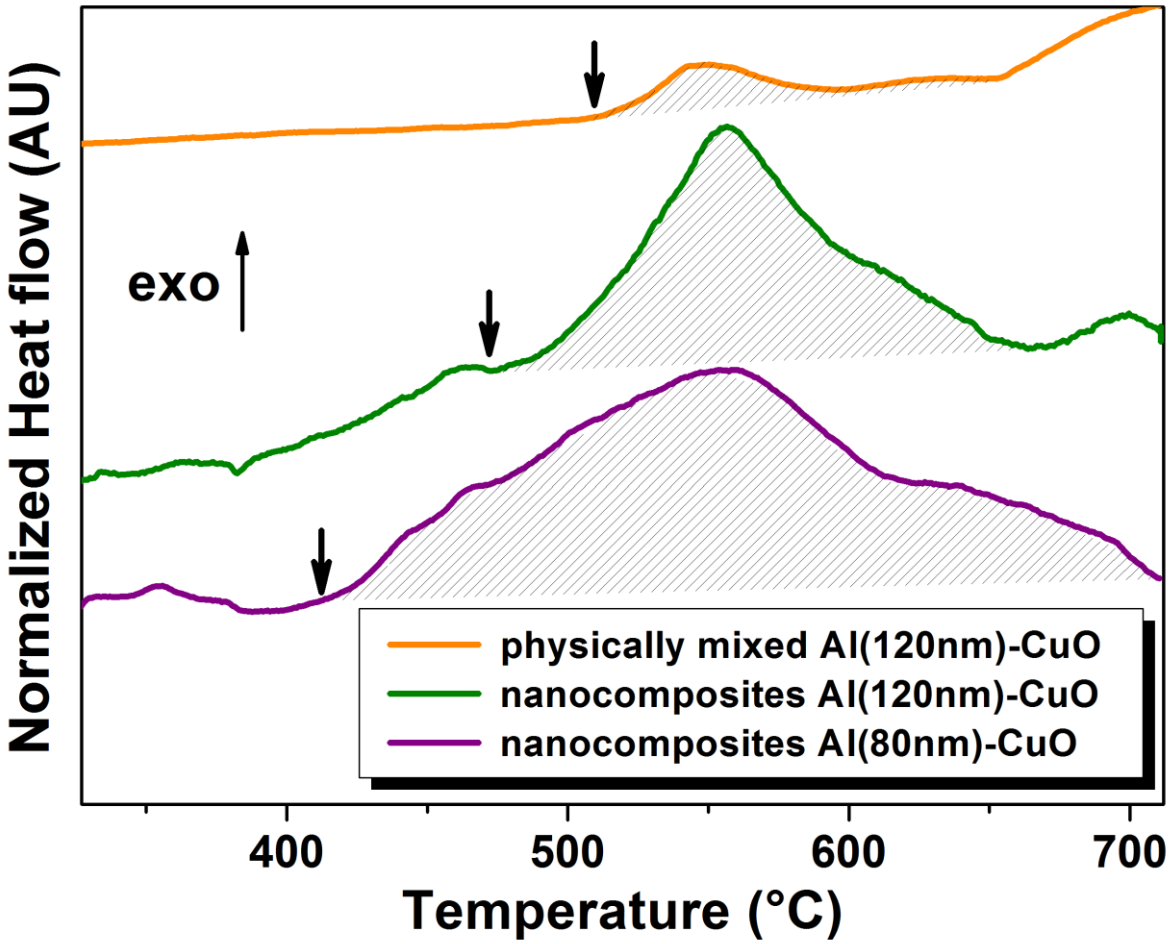

Figure 5. Energetic characterization of Al/CuO nanocomposites. Differential Scanning Calorimetry curves of Al/CuO aggregates produced by physically mixing of Al (120nm) and CuO nanoparticles (orange), DNA directed assembling of Al (120nm) and CuO nanoparticles (green), and DNA directed assembling of Al (80nm) and CuO NPs (purple). Note that the actual size of Al nanoparticles differs from the specifications, as shown in Fig. 3b. Heats of reaction are determined by the integration of the exotherm (hatched area), and onset temperatures are indicated by vertical arrows. DSC scans were performed at 5 K/min under N_2 atmosphere.

DNA	Sequence (5’ to 3’)	Concentration
ssA	SH - $(A)_{20}$**CATACTGTACGTTAA**	500µM
ssB	SH - $(A)_{20}$**TTAACGTACAGTATG**	500µM
ssC	SH - $(A)_{20}$ **CTCCCTAATAACAAT**	500µM
ssA_b	Biotin- $(A)_{20}$**CATACTGTACGTTAA**	500µM
ssB_b	Biotin- $(A)_{20}$**TTAACGTACAGTATG**	500µM
ssC_b	Biotin- $(A)_{20}$**CTCCCTAATAACAAT**	500µM
Linker	**GAGGGATTATTGTTATTAACGTACAGTATG**	500µM

Table 1: List of DNA sequences, complementary sequences are color coded.

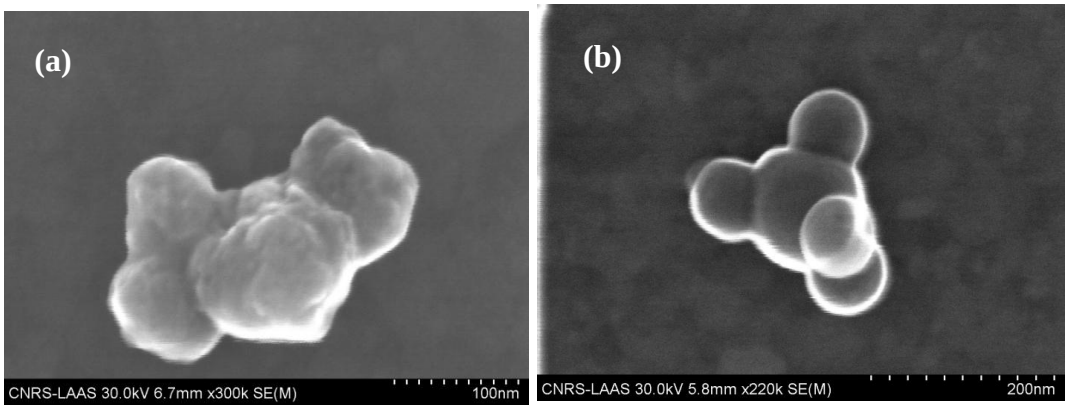

Figure S1. SEM pictures of small indivisibles aggregates of CuO (a) and Al (b) nanoparticles after suspending nanopowders.

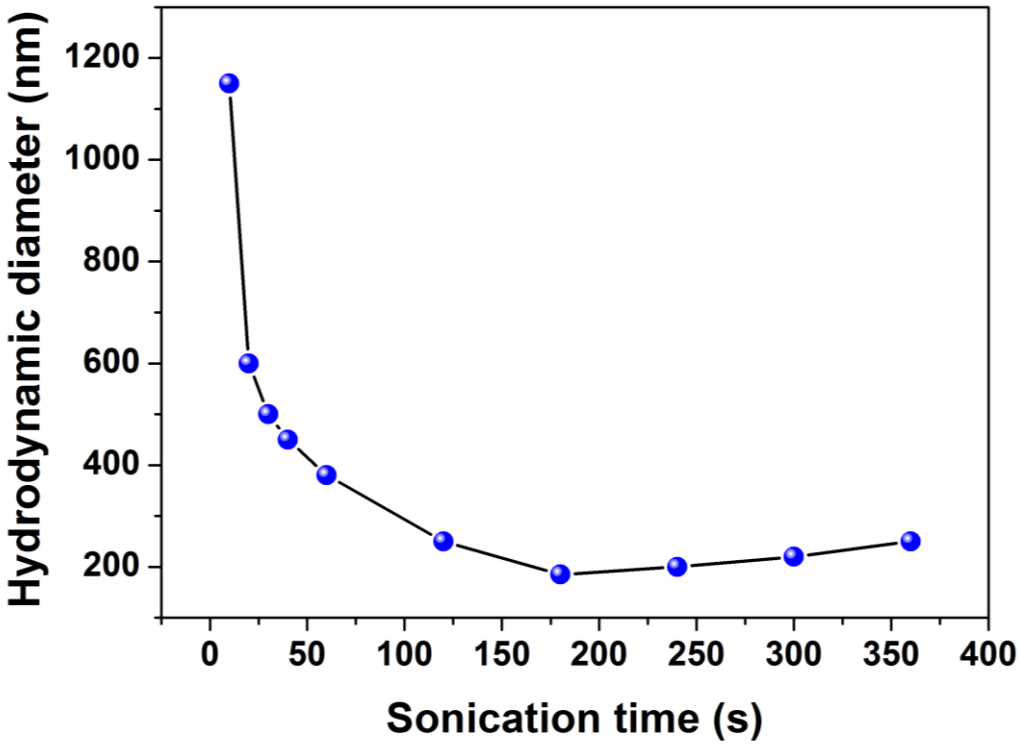

Figure S2. CuO nanoparticles size function of sonication time, longer periods of sonication did not reduce the size of these aggregates, and rather produced colloidal suspensions of larger dimensions.

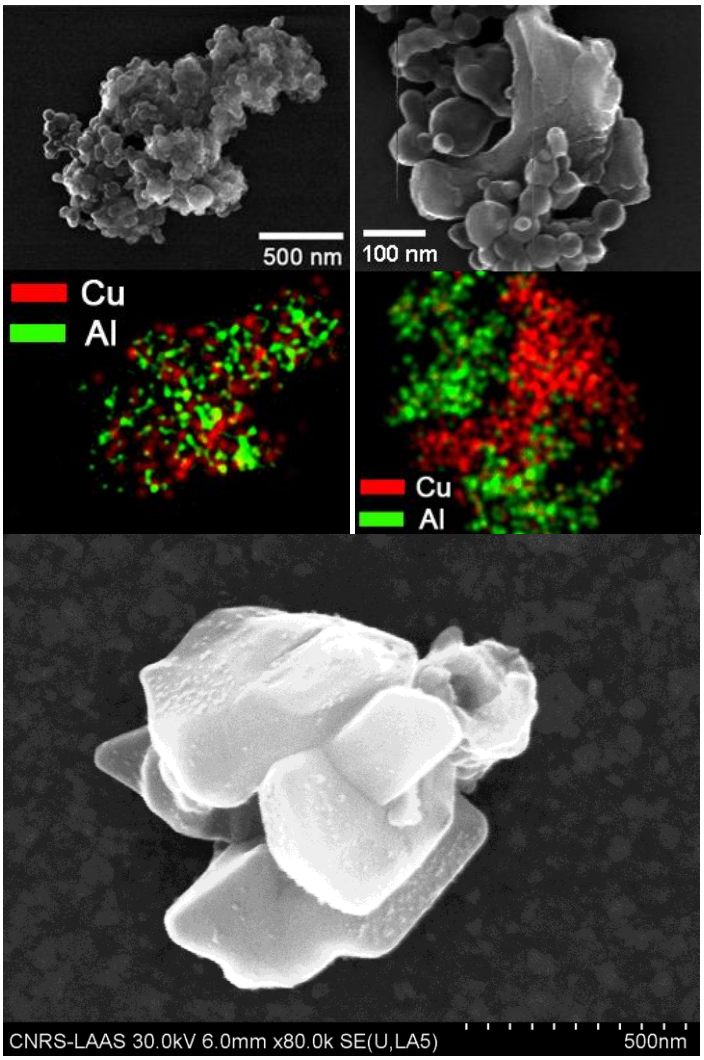

Figure S3. Spatially resolved SEM-EDX analysis was performed on large scale aggregates to show that Cu and Al are randomly present in aggregates **(upper left panel)**. Note that the resolution of SEM-EDX of ~1 µm in thickness does not allow to observe individual NPs in these large aggregates. The same experiment was carried out on small aggregates obtained at the early stage of aggregation **(upper right panel)**. The morphological inspection of the SEM shows small spherical particles surrounding a large multi-facetted particle. Given that the analysis of CuO NPs demonstrated their facetted appearances **(lower panel)** in comparison to Al NPs **(Supplementary Fig. S1b)**, this micrograph indicates the random mixing of both types of NPs in individual clusters.

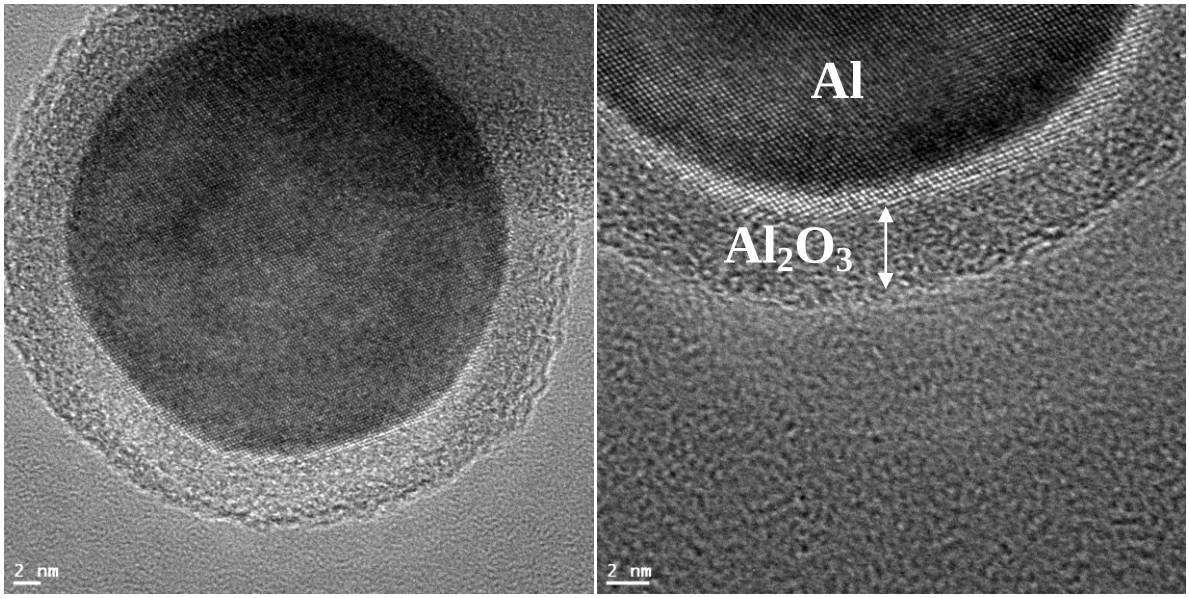

Figure S4. TEM photographs clearly show a 3-4 nm alumina (Al_2O_3) passivation shell around the reactive Al after 1 hour in aqueous solution: the calculation of oxide shell thickness from purity data given by manufacturer (75%) is 3.30nm and 4.95nm for 80nm and 120nm aluminum nanoparticle respectively. Data is not shown for 80 nm nanopowders but stability is the same.